Organic & Biomolecular Chemistry

ROYAL SOCIETY OF CHEMISTRY

PAPER

Cite this: *Org. Biomol. Chem.*, 2024, **22**, 7425

A molecular electron density theory study of the bimolecular nucleophilic substitution reactions on monosubstituted methyl compounds†

Luis R. Domingo, *[a] Patricia Pérez, [b] Mar Ríos-Gutiérrez [a] and M. José Aurell [a]

Received 5th July 2024,
Accepted 15th August 2024

DOI: 10.1039/d4ob01113a

rsc.li/obc

The nucleophilic substitution reactions involving methyl monosubstituted compounds have been studied within the Molecular Electron Density Theory (MEDT) at the ωB97X-D/6-311+G(d,p) computational level in DMSO. This study aims to characterize the electronic nature of the transition state structures (TSs) involved in the so-called S_N2 and S_Ni reactions. Both electron localization function and atom-in-molecules topological analyses indicate that the TSs involved in these nucleophilic substitutions can be described as a central methyl CH_3^+ carbocation, which is strongly stabilized by the presence of two neighbouring nucleophilic species through electron density transfer. This MEDT study establishes a significant electronic similarity between the so-called S_N1 and S_N2 reactions. Due to the weak electrophilic character of the methyl tetrahedral carbons, the departure of the leaving group should be expected with the approach of the nucleophile. However, while along the S_N1 reactions, the strong stabilization of the tertiary carbocation does not demand the participation of the nucleophile, along the S_N2 and S_Ni reactions involving primary tetrahedral carbons, the nucleophiles should participate in the reaction to stabilize the unstable methyl carbocation.

1. Introduction

Nucleophilic substitutions are fundamental reactions of broad synthetic and academic interest. An interpretation that laid the basis for current understanding was developed by C. K. Ingold and E. D. Hughes in the 1930s.[1–3]

Nucleophilic substitution reactions may involve several different combinations of charged and uncharged species as reactants. Scheme 1 shows the four most common reaction types.[4]

Two limiting mechanisms, defined by Hughes and Ingold,[1] namely the ionization mechanism (S_N1, or unimolecular nucleophilic substitution) and the direct displacement mechanism (S_N2, bimolecular nucleophilic substitution) were established (see Scheme 2). While a stepwise mechanism with the formation of a carbocation intermediate in the rate-determining step was proposed for the S_N1 reaction, a concerted mechanism *via* a single rate-determining transition state structure (TS) was proposed for the S_N2 reactions (see Scheme 2). According to the concerted mechanism, the reactant was proposed to be bonded to a nucleophile from the side opposite the leaving group (LG), with bond-making and bond-breaking occurring simultaneously.

Based on the outdated frontier molecular orbital (FMO) theory,[5] the central carbon at **TSc** should have a trigonal bipyramidal geometry with a pentacoordinate carbon (see Fig. 1).

The nucleophilic substitution reactions have been extensively studied over the years,[4,6] being widely studied from a

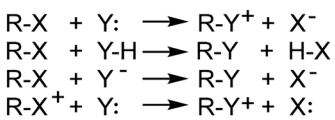

Scheme 1 The four most common nucleophilic substitution reaction types involving charged and uncharged species.

[a]*Department of Organic Chemistry, University of Valencia, Dr. Moliner 50, 46100 Burjassot, Valencia, Spain. E-mail: luisrdomingo@gmail.com*
[b]*Universidad Andrés Bello, Facultad de Ciencias Exactas, Departamento de Ciencias Químicas, Centro de Química Teórica & Computacional, Av. República 275, 8370146, Chile*

†Electronic supplementary information (ESI) available: Fig. S1 with the representations of the contour line maps of the Laplacian $\nabla^2\rho(r)$ of the electron density at the methyl **8** and *tert*-butyl **9** carbocations. Fig. S2 with the ωB97X-D/6-311+G(d,p) Geometries of the selected points of the scans for the C···OH_2 breaking bond in the reactions of protonated methanol **4** and *tert*-butanol **14**. Table S1 with ωB97X-D/6-311+G(d,p) total energies in DMSO of the stationary points involved in the S_N2 reactions of methyl-substituted compounds **1–4**, and in the S_Ni reaction of **6**. ωB97XD/6-311+G(d,p) computed total energies, imaginary frequencies, and Cartesian coordinates, in DMSO, of the stationary points involved in the S_N2 reactions of methyl-substituted compounds **1–4**, and in the S_Ni reaction of **6**. See DOI: https://doi.org/10.1039/d4ob01113a

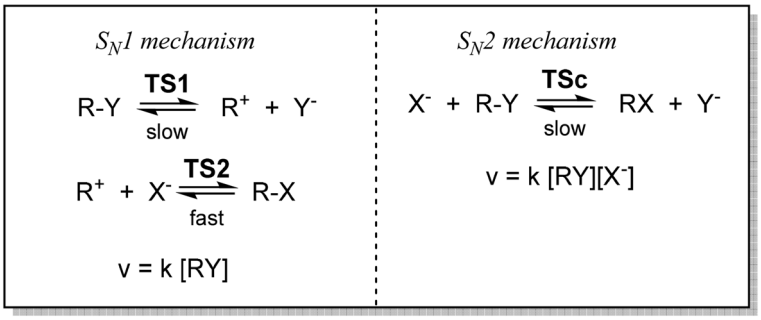

Scheme 2 Two limiting mechanisms, S_N1 and S_N2, for the nucleophilic substitution reactions.

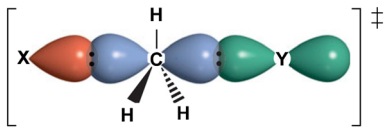

TSc

Fig. 1 Proposed concerted **TSc** for the S_N2 reactions, involving a pentacoordinate carbon, based on the frontier molecular theory.

theoretical point of view.[7–22] Bickelhaupt and coworkers have studied extensively the S_N2 reactions.[18–20] In 2009, Bickelhaupt *et al.* proposed the feasible existence of a labile hypervalent carbon atom at the TSs of the S_N2 reactions.[20]

In 2008, Andrés *et al.*[22] reported a theoretical study based on the electron localization function[23] (ELF) and catastrophe theory[24] analyses for the forming/breaking bond processes and electronic rearrangements along the reaction path associated with the molecular mechanism for the gas-phase symmetric $XCH_3 + X^-$ (X = F, Cl, Br) S_N2 reactions. This study highlighted that in these symmetric S_N2 reactions, the TSs were characterized by ionic species and lacked a disynaptic basin connecting the halogens and the central carbon atom. This gas-phase ELF analysis contrasts with the widely accepted mechanism in which the breaking/forming bonds in an S_N2 reaction take place through a concerted mechanism involving a pentacoordinated TS (see Fig. 1).

Due to the importance of adequately characterizing the TSs associated with S_N2 reactions involving methyl-substituted compounds and thus understanding their molecular mechanisms from an electronic standpoint, a Molecular Electron Density Theory[25] (MEDT) study of six intermolecular S_N2 reactions of three methyl-substituted compounds **1–3**, *i.e.*, two symmetric reactions (i and ii), and four asymmetric reactions (iii–vi) (see Scheme 3), and the intramolecular nucleophilic substitution reaction (S_Ni) of 5-chloro-*N*,*N*-dimethylpentan-1-amine (CPA **6**) (see vii in Scheme 4), have been herein carried out. Note that S_Ni reactions have a first-order kinetic equation $v = k$ [X–RY] similar to the S_N1 ones (see Scheme 2). Due to the relevance of polar solvents in nucleophilic substitution reactions as a consequence of the participation of different charged species in the reaction, the present MEDT study has been carried out in dimethyl sulfoxide (DMSO) or water. To

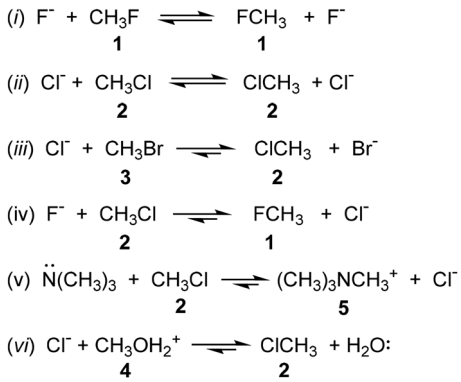

Scheme 3 S_N2 reactions of the methyl-substituted compounds **1–4**.

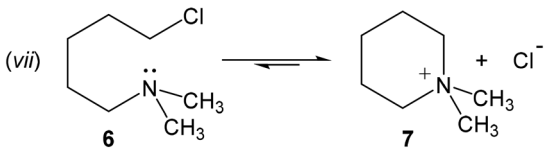

Scheme 4 S_Ni reaction of CPA **6**.

characterize the electronic structure of the TSs, a comparative ELF and Quantum Theory of Atom in Molecules[26,27] (QTAIM) topological analysis on the reagents and the seven TSs involved in these nucleophilic substitution reactions was performed.

2. Results and discussion

The present MEDT study has been organized into six sections: (i) the first section contains the ELF and QTAIM topological analyses of the ground state (GS) electronic structure of the reagents **1–4** involved in the S_N2 reactions; (ii) the second section conducts an analysis of the density functional theory (DFT) reactivity indices at the GS of the reagents; (iii) the third section explores the reaction paths associated with the S_N2 reactions on the methyl-substituted compounds **1–4**; (iv) the fourth section is focused on ELF and QTAIM topological analyses of the TSs associated with these S_N2 reactions; (v) the

fifth section presents a comparative study of the S_Ni reaction of CPA **6** with the previously studied S_N2 reactions; and finally, (vi) the sixth section provides a comparative analysis of the kinetics of the S_N1 and S_N2 reactions.

2.1 ELF and QTAIM analyses of the electronic structures of methyl-substituted compounds 1–4

The topological analysis of the ELF[23] permits a quantitative characterization of the electron density distribution in a molecule,[28] allowing the establishment of a correlation between its electronic structure and reactivity. Thus, an ELF topological analysis of the electronic structures of methyl-substituted compounds **1–4**, used as the substrates in these S_N2 reactions, was performed first. ELF basin attractor positions and the most relevant valence basin populations are shown in Fig. 2.

Upon examination, the ELF of the four methyl-substituted compounds reveals the presence of a V(C,X) disynaptic basin integrating less than 1.30e. This low population arises from the high electronegative character of the X heteroatom compared to the carbon atom, which polarizes the electron density of the C–X region towards the X heteroatom. Consequently, the sum of the population of the V(X) monosynaptic basins at the heteroatoms exceeds the 6*e* for the halogens and the 2*e* for the oxygen (see Vt(X) in Fig. 2).

Finally, a QTAIM[26,27] topological analysis of the electron density ρ at the C–X interacting region of the four methyl-substituted compounds **1–4** was performed. Contour line maps of the Laplacian $\nabla^2\rho(r)$ of the electron density are shown in Fig. 3, while the calculated QTAIM parameters of the (3,–1) bond critical points (CPs) associated with the C–X bonding region are provided in Table 1.

Interestingly, in methyl derivatives involving the most electronegative F atom, CH_3F **1**, and the positively charged $-OH_2^+$ group, $CH_3OH_2^+$ **4**, the Laplacian $\nabla^2\rho(r)$ shows a positive value, indicating the absence of any covalent interaction. However, in the CH_3Cl **2** and CH_3Br **3** compounds, $\nabla^2\rho(r)$ shows a negative value, indicating the presence of a covalent interaction as the electron density is located in that region.

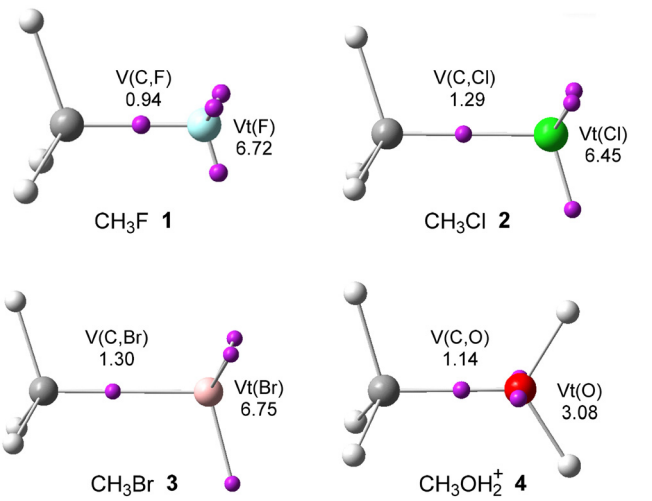

Fig. 2 ωB97X-D/6-311+G(d,p) ELF basin attractor positions, populations of the C–X valence basins, and the sum of the population of the V(X) monosynaptic basins at the heteroatoms of methyl-substituted compounds **1–4**. Valence basin populations are given in average number of electrons, *e*.

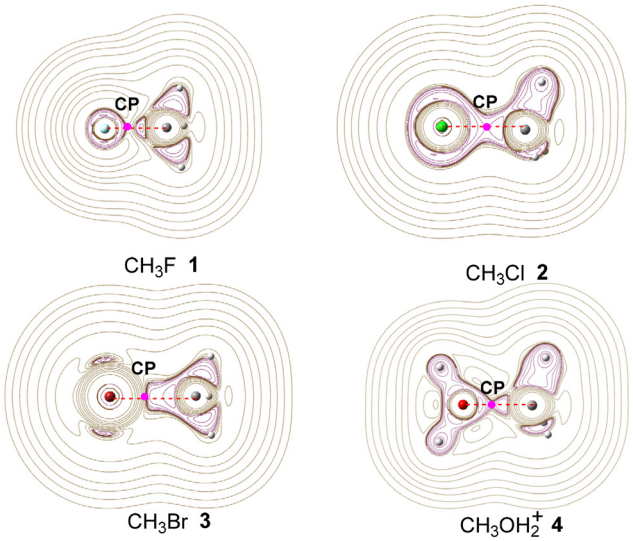

Fig. 3 Representations of the contour line maps of the Laplacian $\nabla^2\rho(r)$ of the electron density at four methyl-substituted compounds **1–4**. The critical points **CP** are colored in pink, while the bond path is in red.

Table 1 ωB97X-D/6-311+G(d,p) QTAIM parameters, in atomic units (a.u.) for the (3,–1) bonding CPs in the C–X interacting regions of the four methyl-substituted compounds **1–4**

CP	C–F	C–Cl	C–Br	C–OH_2^+
Density	0.2326	0.1788	0.1488	0.1773
Laplacian	0.0919	−0.2350	−0.1424	0.1981
$G(r)$	0.3230	0.0589	0.0467	0.2564
$K(r)$	0.3000	0.1177	0.0823	0.2067
$V(r)$	−0.6230	−0.1766	−0.1290	−0.4631
$\lvert V(r)\rvert/G(r)$	1.9288	2.9965	2.7618	1.8063

Espinosa[29] proposed a useful criterion to characterize interactions at the CPs using an analysis of the ratio of the potential and kinetic energy electron density $|V(r)|/G(r)$. For ionic, non-covalent, and HB interactions, $|V(r)|/G(r) < 1$. Non-covalent interactions with somewhat covalent characters are characterized by $1 < |V(r)|/G(r) < 2$, while covalent interactions show $|V(r)|/G(r) > 2$. The calculated values of $|V(r)|/G(r)$ at the selected CPs are given in Table 1. While for the CH_3F **1** and $CH_3OH_2^+$ **4** compounds the $|V(r)|/G(r)$ values, 1.93 and 1.81, respectively, indicate that the corresponding C–X bonds have a non-covalent interaction with somewhat covalent character, for the CH_3Cl **2** and CH_3Br **3** compounds the $|V(r)|/G(r)$ values >2.00 indicate that the corresponding C–X bonds have a covalent nature.

2.2. Analysis of the reactivity indices at the GS of the reagents

The analysis of the DFT reactivity indices[30,31] at the GS of the reagents is a powerful tool for understanding the reactivity in

polar reactions.[32] The reactivity indices were calculated at the ωB97X-D/6-311+G(d,p) computational level. A recent study has shown that there are excellent linear correlations between the reactivity indices obtained at different levels of calculation with those obtained at the B3LYP/6-31G(d) level.[33] Due to the strong electrophilic and nucleophilic character of the charged species, the reactivity indices were calculated in DMSO. The global reactivity indices, namely, the electronic chemical potential μ, chemical hardness η, global electrophilicity ω, and global nucleophilicity N, for the methyl-substituted compounds **1–4** and CPA **6** are given in Table 2, while those for the nucleophilic reagents are provided in Table 3.

Analysis of the electrophilicity ω indices of the methyl-substituted compounds **1–4** indicates that, except for protonated methanol $CH_3OH_2^+$ **4**, which is positively charged, the other methyl derivatives have electrophilicity ω indices lower than 0.87 eV, thus being classified as moderate electrophiles. CPA **6** is the least electrophilic species of this series due to the presence of the electron-releasing (ER) methylene group attached to the $-CH_2Cl$ moiety. On the other hand, the presence of the tertiary amine group in CPA **6** makes this compound a strong nucleophilic species with N = 2.86 eV.

The methyl carbocation **8** is a superelectrophile, ω = 4.61 eV. The presence of three ER methyl groups in *tert*-butyl carbocation **9** markedly decreases the electrophilic character of this species, ω = 2.61 eV.

The presence of three ER methyl groups in protonated *tert*-butanol $C(CH_3)_3OH_2^+$ **10** and *tert*-butyl chloride $C(CH_3)_3Cl$ **11** slightly decreases the electrophilicity of protonated methanol $CH_3OH_2^+$ **4** and methyl chloride **2**, $\Delta\omega$ = −0.17 and −0.01 eV, respectively. Note that in the case of the methyl carbocation **8** the corresponding decrease is −2.00 eV. This behavior is a consequence of the poor electrophilic character of the saturated tetrahedral carbon; note that the electrophilicity ω index of methane **12** is 1.01 eV (see Table 2).

Analysis of the nucleophilicity N indices of the nucleophilic reagents indicates that trimethylamine NMe_3 is the most nucleophilic of this series. As expected, the halides series follows the Br > Cl > F order.

In 2006, Pérez *et al.*[34] proposed a scale of the nucleofugacity for leaving groups (LG) based on the electrophilicity ω index of the CH_3-LG molecules computed at the B3LYP/6-31G*(d) computational level in the gas phase. As expected, the estimated nucleofugacity of these LG groups was ordered as $-OH_2^+$ (ω = 6.47 eV) ≫ –Br (ω = 0.90 eV) > –Cl (ω = 0.77 eV) > –F (ω = 0.40 eV).[34]

2.3. Analysis of the reaction paths associated with the S_N2 reactions on the methyl-substituted compounds 1–4

To analyze the electronic structure of the TSs involved in S_N2 reactions on the methyl-substituted compounds **1–4** and thus characterize the molecular mechanism from an electronic point of view, six S_N2 reactions (i–vi) were studied (see Scheme 3). In two reactions, the nucleophile and the LG are the same species (symmetric S_N2 reactions i and ii), and in the other four reactions, the two species are different. In each S_N2 reaction, two reagents, one TS, and two products were located and characterized. Consequently, all these intermolecular S_N2 reactions take place through a one-step mechanism. Due to the presence of negatively charged species, all calculations were done in DMSO. All S_N2 reactions can be considered reversible with the direction of the reactions corresponding to the exothermic processes. The ωB97X-D/6-311+G(d,p) relative energies in DMSO are given in Table 4, while the total energies are given in Table S1 in ESI.†

Along the six S_N2 reactions, a series of molecular complexes (MCs) can be found at the beginning and the end of the reaction paths on the potential energy surfaces. Although these MCs have some significance in vacuum calculations, they are not relevant in DMSO.

Some relevant conclusions can be obtained from the relative energies given in Table 4; (i) while the S_N2 reactions i and

Table 2 ωB97X-D/6-311+G(d,p) electronic chemical potential μ, chemical hardness η, electrophilicity ω, and nucleophilicity N, in eV, for the methyl-substituted compounds **1–4**, CPA **6**, and methyl CH_3^+ **8** and *tert*-butyl $C(CH_3)_3^+$ **9** carbocations, in DMSO

	μ	η	ω	N
CH_3^+ **8**	−10.97	13.05	4.61	−6.41
$C(CH_3)_3^+$ **9**	−7.78	11.63	2.61	−2.52
$CH_3OH_2^+$ **4**	−6.23	14.48	1.34	1.09
$C(CH_3)_3OH_2^+$ **10**	−5.68	13.75	1.17	−1.47
CH_4 **12**	−5.5	14.93	1.01	−1.88
CH_3F **1**	−4.94	14.05	0.87	0.50
CH_3Br **3**	−4.35	11.27	0.84	−0.88
CH_3Cl **2**	−4.38	12.41	0.77	−2.39
$C(CH_3)_3Cl$ **11**	−4.31	12.19	0.76	0.67
CPA **6**	−3.25	9.94	0.53	2.86

Table 3 ωB97X-D/6-311+G(d,p) electronic chemical potential μ, chemical hardness η, electrophilicity ω, and nucleophilicity N, in eV, for the nucleophiles, computed in DMSO

Nucleophiles	μ	η	ω	N
NMe_3	−3.18	10.04	0.50	2.88
Br^-	−3.28	10.39	0.52	2.61
Cl^-	−3.11	11.58	0.42	2.18
F^-	−1.46	15.53	0.07	1.86

Table 4 ωB97X-D/6-311+G(d,p) relative energies, in kcal mol^{-1}, in DMSO of the stationary points involved in the S_N2 reactions of methyl-substituted compounds **1–4**

	$F^- + CH_3F$	$Cl^- + CH_3Cl$	$Cl^- + CH_3Br$
R	0.0	0.0	0.0
TS	20.5	21.3	19.4
P	0.0	0.0	−2.2
	$F^- + CH_3Cl$	$NMe_3 + CH_3Cl$	$Cl^- + CH_3OH_2^+$
R	0.0	0.0	0.0
TS	12.8	10.6	5.4
P	−19.6	−25.2	−25.5

ii are isothermic reactions, iii is somewhat exothermic, with $\Delta E = -2.2$ kcal mol^{-1}. Reactions iv, v and vi are strongly exothermic, with $\Delta E < -20.0$ kcal mol^{-1}, and therefore irreversible; (ii) activation energies vary widely, ranging between 20.5 (i) and 5.4 (vi) kcal mol^{-1}. The activation energies of these S_N2 reactions depend mainly on the nucleophilic character of the nucleophile and the nucleofugacity of the LG. Finally, (iii) the reduction of the activation energy in this series of S_N2 reactions is accompanied by an increase in the exothermic character of the reaction.

The optimized geometries of the six TSs are given in Fig. 4. While **TS-1** and **TS-2** are symmetric because the nucleophile and the LG are the same species, the other four TSs are somewhat asynchronous. At these TSs, the Nu–C and C–LG distances cannot be used to measure the asynchronicity of the breaking/forming bond processes, as these distances are dissimilar in reagents and products. However, the evolution of these S_N2 reactions can be analyzed considering the H–C–H bond angle of the methyl group at the TSs. While at the GS of the reagents, this angle has a value near 109 degrees, according to a tetrahedral carbon, at the symmetric TSs, its value is 120 degrees, according to a trigonal planar carbon. Thus, while at **TS-1** – **TS-3**, this bond angle is 120 degrees, indicating that the central carbon has a trigonal planar structure, at **TS-4** – **TS-6**, the corresponding bond angles are only close to the trigonal planar structure, 119.7 degrees. Thus, the three more favorable reactions are only slightly more delayed.

Next, the global electron density transfer[35] (GEDT) taking place at the TSs of these nucleophilic substitution reactions was evaluated. Recently, it has been showed that the GEDT has a decisive role in polar organic reactions.[36] In a polar TS, there is a GEDT from the nucleophilic to the electrophilic species as a consequence of the difference in electronic chemical potentials μ of these species. The sum of the natural population analysis (NPA) charges of the atoms belonging to the CH_3 framework is given in Fig. 4. The CH_3 framework at the six TSs exhibits a trigonal planar structure. As shown in Fig. 4, the charge of the CH_3 framework ranges from 0.47 (**TS-1**) to 0.29*e* (**TS-3**). The deviation of the total charge from that of the methyl carbocation **8**, 1.00*e*, results from the electron density transferred occurring from the two neighboring X^- and Y^- nucleophilic species toward the electrophilic central methyl carbocation **8**. Thus, at the symmetric **TS-1** and **TS-2**, in which the nucleophile and the LG are the same species, the NPA charges at the F^- and Cl^- anions are −0.73 and −0.66*e*, respectively. The deviation of the charge −1 of these anionic species, 0.27*e* at F^- and 0.34*e* at Cl^-, is a consequence of loss of electron density due to the GEDT occurring from these nucleophilic species to the central superelectrophilic methyl carbocation **8** (see Table 2).

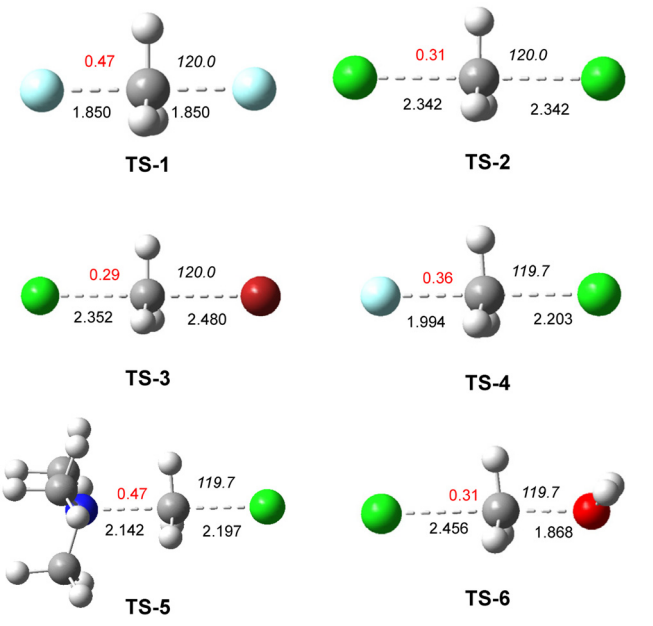

Fig. 4 ωB97X-D/6-311+G(d,p) optimized geometries of the TSs. Distances are given in angstroms Å, while bond angles are given degrees. The sum of the NPA charges at the CH_3 framework, in average number of electrons, *e*, are given in red.

2.4. ELF and QTAIM topological analyses of the TSs associated with the S_N2 reactions on the methyl-substituted compounds 1–4

In this section, ELF and QTAIM topological analyses of the electronic structure of the six TSs were performed in order to characterize the evolution of the rupture and formation of the single bonds at these TSs. Fig. 5 shows the ELF basin attractor positions, together with the most relevant valence basin populations, of the six TSs.

Interestingly, the ELF of the six TSs shows the presence of one V(X) monosynaptic basin in the X–C interacting region, and one V(Y) monosynaptic basin in the C–Y interacting region. Only the nucleophilic fluorine atom does not present the corresponding V(F) monosynaptic basin at **TS-4**. No V(X,C) disynaptic basins are observed in any TS, indicating that while the C–Y single bond has been broken, the formation of the new X–C single has not yet begun. In all TSs, the population of these V(X) monosynaptic basins present a value in the range of 0.3 to 0.6*e*. Only the V(N) monosynaptic basin of nucleophilic trimethyl amine in **TS-5** and the V(O) monosynaptic basin of the LG water at **TS-6** present a population of 1.93 and 1.59*e*, respectively, as these V(X) monosynaptic basins are associated with the nitrogen and oxygen non-bonding electron density present at the trimethyl amine and water nucleophilic molecules.

Next, a QTAIM topological analysis of the six TSs was performed. The positions of the critical points (3,−1) of the electron density ρ are shown in Fig. 6, while the calculated QTAIM parameters are given in Table 5. A representation of the contour line maps of the Laplacian $\nabla^2\rho(r)$ of the electron density at the most unfavourable **TS1** and the most favourable **TS6** is shown in Fig. 7.

As expected, the electron density ρ at the twelve CPs, $\rho <$ 0.08*e*, is noticeably lower than that at the CPs associated with the C–X single bonds at the GS of the reagents, $\rho > 0.15e$ (see Table 1). The Laplacian $\nabla^2\rho(r)$ of the twelve CPs show positive

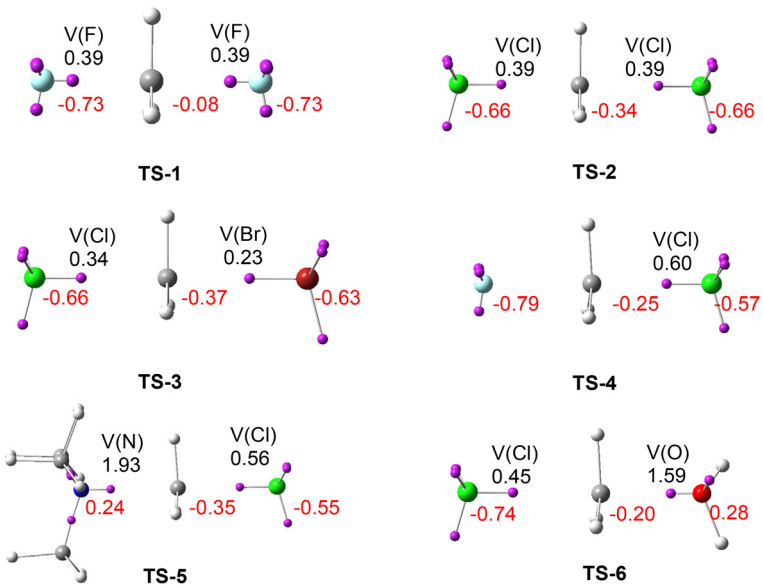

Fig. 5 ωB97X-D/6-311+G(d,p) ELF basin attractor positions and populations of the most relevant valence basins, in average number of electrons, *e*, of the six TSs associated with the intermolecular S_N2 reactions on the methyl-substituted compounds **1–4**. The NPA charges at the interacting atoms are given in red in average number of electrons, *e*.

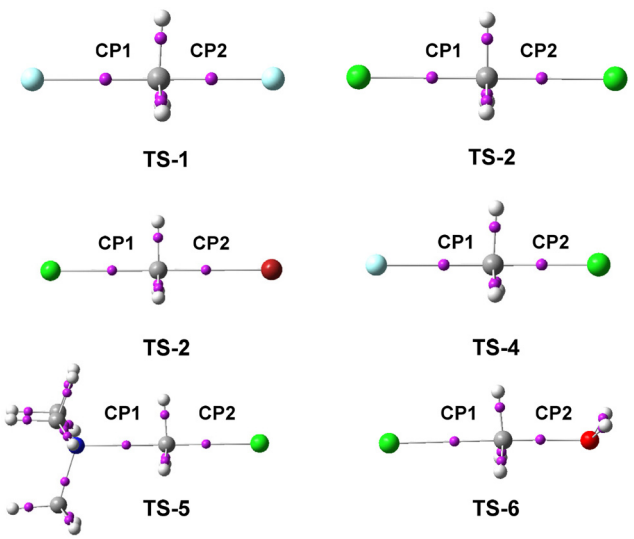

Fig. 6 ωB97X-D/6-311+G(d,p) representation of the CPs (3,–1), in pink, at the six TSs associated with the intermolecular S_N2 reactions on the methyl-substituted compounds **1–4**. The **CP1** associated with the Nu···C interacting region and the **CP2** associated with the C···LG interacting region are labelled.

values, indicating the absence of any covalent interaction. The calculated $|V(r)|/G(r)$ values, which are lower than 1.52, suggest that, according to the Espinosa criteria,[29] the corresponding C–X(Y) interactions have a non-covalent interaction with somewhat covalent character.

Finally, a comparison of the contour line maps of the Laplacian $\nabla^2\rho(r)$ of **TS1** and **TS6** given in Fig. 7 with those of the corresponding methyl-substituted molecules given in Fig. 2, shows that the central CH_3 framework at these TSs has the electronic structure of the methyl carbocation **8** given in Fig. S1 in ESI.†

Consequently, we can conclude that in the six S_N2 reactions, the electronic structure of the central CH_3 framework at the six TSs is that of the methyl carbocation **8**, strongly electronically stabilized by the GEDT, taking place from the two neighboring nucleophilic species. Thus, the activation energies of these S_N2 reactions can be related to the electronic stabilization of the incipient methyl carbocation **8** by the presence of the two nucleophilic species.

2.5. Study of the S_Ni reaction of CPA 6

The S_Ni reaction of CPA **6** was studied to conduct a comparative analysis between the inter and intramolecular nucleophilic substitution reactions. Note that S_Ni reactions have a first-order kinetics similar to S_N1 reactions, *i.e.*, $v = k$ [X–RY] (see Scheme 2). The ωB97X-D/6-311+G(d,p) relative energies in DMSO are given in Table 6, while the total energies are given in Table S1 in ESI.†

The activation energy associated with this S_Ni reaction is 13.1 kcal mol^{-1}, the reaction being exothermic by −25.3 kcal mol^{-1}. When comparing these relative energies with those of the intermolecular S_N2 process, the activation energy associated with **TS-7** is *ca.* 2.5 kcal mol^{-1} higher than that associated with **TS-5**. This energy difference can be attributed to the lower electrophilic character of CPA **6** compared to that of methyl chloride **2** (see Table 2), and to some geometrical constraints associated with the intramolecular process (see later). However, both reactions exhibit a similar exothermic character (see Tables 4 and 6).

Table 5 ωB97X-D/6-311+G(d,p) QTAIM parameters, in atomic units a.u., of the (3,–1) CPs **CP1** and **CP2** at the six TSs associated with the intermolecular S_N2 reactions on the methyl-substituted compounds **1–4**

	TS-1		TS-2		TS-3	
	CP1	**CP2**	**CP1**	**CP2**	**CP1**	**CP2**
Density $\rho(r)$	0.0770	0.0770	0.0502	0.0502	0.0494	0.0463
Laplacian $\nabla^2\rho(r)$	0.1864	0.1864	0.0806	0.0806	0.0805	0.0625
$G(r)$	0.0614	0.0614	0.0274	0.0274	0.0270	0.0225
$K(r)$	0.0148	0.0148	0.0073	0.0073	0.0069	0.0069
$V(r)$	−0.0762	−0.0762	−0.0347	−0.0347	−0.0339	−0.0294
$\lvert V(r)\rvert/G(r)$	1.2408	1.2408	1.2651	1.2651	1.2545	1.3054
	TS-4		**TS-5**		**TS-6**	
	CP1	**CP2**	**CP1**	**CP2**	**CP1**	**CP2**
Density $\rho(r)$	0.0561	0.0682	0.0384	0.0807	0.0576	0.0703
Laplacian $\nabla^2\rho(r)$	0.1706	0.0659	0.0822	0.1487	0.1118	0.0657
$G(r)$	0.0465	0.0338	0.0233	0.0587	0.0363	0.0343
$K(r)$	0.0039	0.0173	0.0028	0.0215	0.0083	0.0179
$V(r)$	−0.0504	−0.0510	−0.0261	−0.0802	−0.0446	−0.0522
$\lvert V(r)\rvert/G(r)$	1.0832	1.5117	1.1190	1.3667	1.2294	1.5217

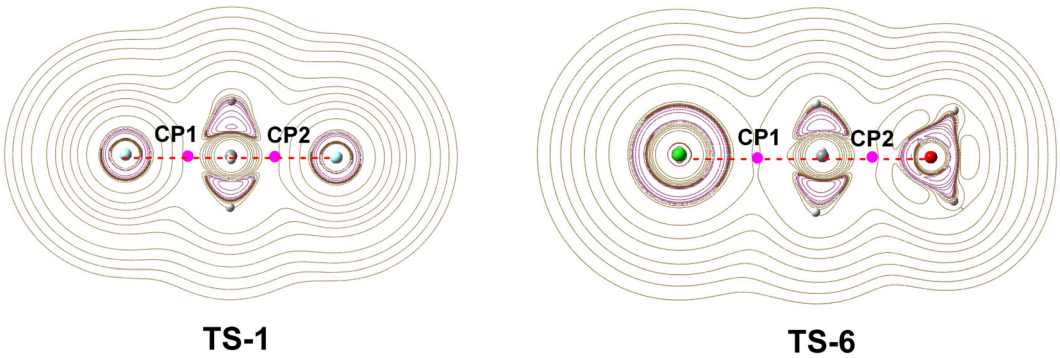

Fig. 7 Representations of the contour line maps of the Laplacian $\nabla^2\rho(r)$ of the electron density at the most unfavourable **TS-1** and the most favourable **TS-6**. The critical points **CP** are marked in pink, while the bond path is in red.

Table 6 ωB97X-D/6-311+G(d,p) relative energies, in kcal mol^{-1}, in DMSO of the stationary points involved in the S_Ni reaction of CPA **6**

	ΔE
CPA **6**	0.0
TS-7	13.1
7	−25.3

The optimized geometry of **TS-7** is given in Fig. 8. The N–C and C–Cl distances at this TS are 2.243 and 2.264 Å, respectively. These distances are slightly longer than those at **TS-5** associated with the intermolecular process (see Fig. 4). On the other hand, while the N–C–Cl bond angle in the intermolecular process is nearly 180 degrees, it is 162.4 degrees at **TS-7**. These geometric variations may be due to geometric constraints associated with the intramolecular process. These geometrical constraints and the lower electrophilic character of CPA **6**, compared to methyl chloride **2**, can account for the higher activation energy associated with **TS-7**.

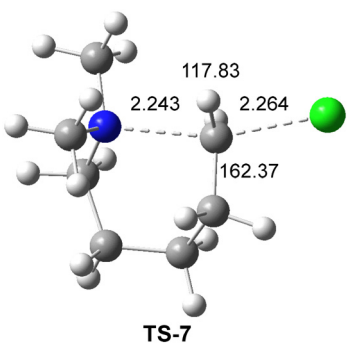

Fig. 8 ωB97X-D/6-311+G(d,p) optimized geometries of **TS-7**. Distances are given in angstroms Å, while bond angles are given in degrees.

Finally, an ELF and QTAIM topological analysis of the electron density of **TS-7** was performed. ELF basin attractor positions, along with the most relevant valence basin populations of **TS-7**, are shown in Fig. 9. ELF analysis of **TS-7** shows the

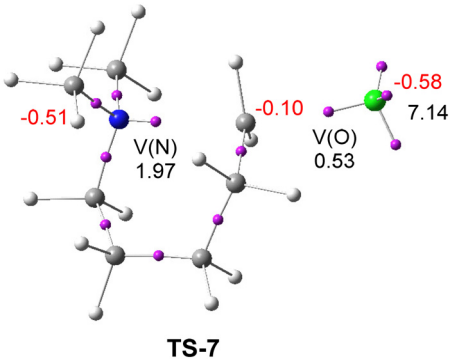

Fig. 9 ωB97X-D/6-311+G(d,p) ELF basin attractor positions, populations of the valence basins in the C–X regions, the sum of the population of the V(Cl) monosynaptic basins, and the NPA charges of the three interacting atoms of **TS-7**. Valence basin populations and natural atomic charges are given in average number of electrons, *e*.

presence of one V(N) monosynaptic basin integrating 1.94*e*, associated with the nitrogen non-bonding electron density of the amine, and a V(Cl) monosynaptic basin integrating 0.53*e* resulting from the C–Cl breaking bond. A comparative ELF analysis of the intermolecular **TS-5** and the intramolecular **TS-7** shows a great similitude (see Fig. 5 and 9).

Next, a QTAIM topological analysis of **TS-7** was performed. The position of the critical points (3,−1) of the electron density ρ are shown in Fig. 10a, while the calculated QTAIM parameters are provided in Table 7. Together with the CPs **CP1** and **CP2** associated with the N···C and C···Cl interacting regions, respectively, a **CP3** associated with a covalent C–C single bond of the linear pentane chain has been selected for a comparative analysis. A representation of the contour line maps of the Laplacian $\nabla^2\rho(r)$ of the electron density is shown in Fig. 10b.

Table 7 ωB97X-D/6-311+G(d,p) QTAIM parameters, in atomic units a.u., of the (3,−1) CPs **CP1**, **CP2** and **CP3** at **TS-7**

	CP1	CP2	CP3
Density	0.0613	0.0472	0.2430
Laplacian	0.0715	0.1032	−0.5557
$G(r)$	0.0308	0.0302	0.0561
$K(r)$	0.0129	0.0044	0.1950
$V(r)$	−0.0437	−0.0346	−0.2512
$\lvert V(r)\rvert/G(r)$	1.4198	1.1452	4.4743

A preliminary comparative QTAIM analysis of the N···C···Cl interacting regions in **TS-5**, associated with the S_N2 reaction, and those in **TS-7**, associated with the S_Ni reaction, shows a great electronic similarity between both TSs. As expected, the electron density ρ at **CP1** and **CP2**, ρ < 0.06*e*, is noticeably lower than at **CP3** associated with the selected C–C single bond, where ρ > 0.24*e* (see Table 1). The Laplacian $\nabla^2\rho(r)$ at **CP1** and **CP2** show positive values, indicating the absence of any covalent interaction, while that at **CP3** is negative, with $\nabla^2\rho(r)$ = −0.56. The calculated $|V(r)|/G(r)$ values at **CP1** and **CP2**, <1.42, indicate that, according to the Espinosa criteria,[29] the corresponding C–X and C–Y interactions have a non-covalent nature with somewhat covalent character. Note that the $|V(r)|/G(r)$ value at **CP3** is 4.47, indicative of a covalent bond.

From this comparative analysis between the electronic behaviors of the TSs involved in the S_Ni and S_N2 reactions, it is possible to conclude that these nucleophilic substitution reactions present a complete similarity. They are characterized by the formation of a methyl carbocation in which the C–Y single bond of the LG is already broken, while the formation of the C–X single bond with the nucleophilic reagent has not begun yet. This electronic behavior of the TSs involved in the S_N2 and S_Ni reactions of methyl-substituted compounds discards the

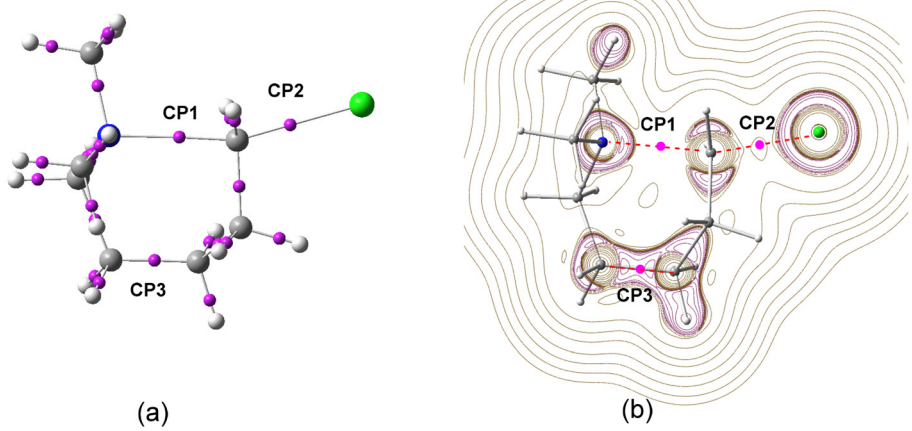

Fig. 10 (a) ωB97X-D/6-311+G(d,p) representation of the CPs (3,−1), in pink, at **TS-7**. The **CP1** associated with the N···C interacting region and the **CP2** associated with the C···Cl interacting region are labelled; (b) representations of the contour line maps of the Laplacian $\nabla^2\rho(r)$ of the electron density of **TS-7**. The critical points **CP1**–**CP3** are marked in pink, while the bond path is in red.

generally accepted concerted mechanism involving a penta-coordinated carbon at the corresponding TS,[20] widely accepted in all textbooks.[4]

2.6. A comparative analysis between the unimolecular S_N1 and bimolecular S_N2 relations

If both S_N2 and the S_N1 reactions take place through the formation of a carbocationic species, why are they kinetically different? The isodesmic reaction[4] given in Scheme 5 shows that in DMSO, the *tert*-butyl carbocation **9** is 67.0 kcal mol^{-1} more stable than the methyl one **8**. On the other hand, the *tert*-butyl carbocation **9**, with ω = 2.61 eV, is half as electrophilic as the methyl one **8**, ω = 4.61 eV (see Table 2). Therefore, the presence of three ER methyl groups in the *tert*-butyl carbocation **9** has two relevant roles in its structure/reactivity: (i) the *tert*-butyl carbocation **9** is strongly stabilized with respect to the methyl carbocation **8**; and (ii) the electrophilic character of the *tert*-butyl carbocation **9** decreases markedly compared to that of the methyl carbocation **8**.

Experimentally, the *tert*-butyl chloride **11** formation from *tert*-butanol **12** and hydrochloric acid takes place quickly at room temperature, while this reaction experimentally does not occur with methanol **13** (see Scheme 6).

Two experiment scans were performed to understand the differing reactivity of the two alcohols (see Fig. 11). The starting points of these scans were the MCs formed by the chloride anion plus the protonated alcohols, **P1-6** for protonated methanol **4** and **P1-8** for protonated *tert*-butanol **14**. Note that in concentrated hydrochloric acid, both alcohols are protonated. Along these scans, the C···OH_2 distances were increased from 1.50 to 2.70 Å, structures **P3-6** and **P3-8**; note that at these points, the C–O single bond is already broken (see later). Some interesting conclusions can be drawn from these scans: (i) while in the reaction with protonated methanol **4**, the energy of the system increases to reach 8.6 kcal mol^{-1} at 1.85 Å, in the reaction with protonated *tert*-butanol **13** it increases to 7.8 kcal mol^{-1} at 2.70 Å; (ii) geometrical optimization of the maximum point of the scan for the reaction of protonated methanol **4** gives the TS of the reaction, **TS-6w**, which

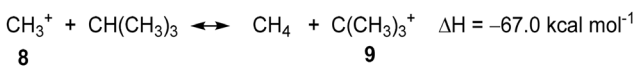

Scheme 5 ωB97X-D/6-311+G(d,p) isodesmic reaction in DMSO showing the strong stabilization of the *tert*-butyl carbocation **9** with respect to the methyl one **8**.

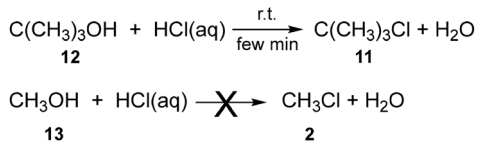

Scheme 6 Reactions of *tert*-butanol **12** and methanol **13** with hydrochloric acid.

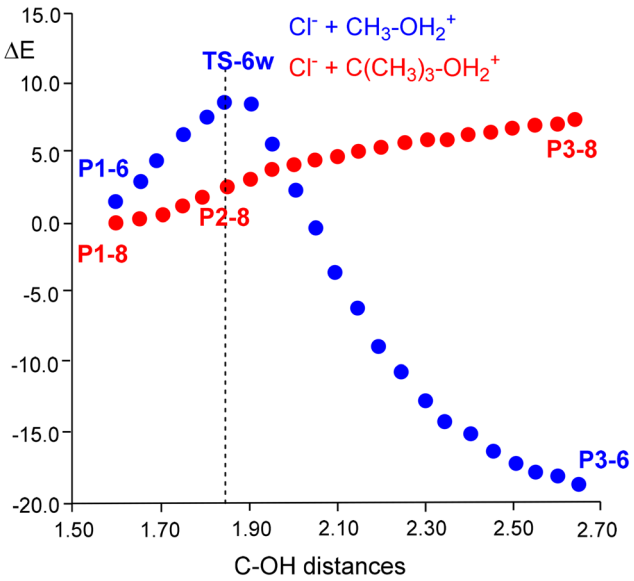

Fig. 11 ωB97X-D/6-311+G(d,p) scans in water for the C···OH_2 breaking bond in the reactions of protonated methanol **4** and protonated *tert*-butanol **14**. Relative energies are given in kcal mol^{-1}.

is 0.34 kcal mol^{-1} more stable than that of **TS-6**, due to higher solvation of the TS in water than in DMSO, (iii) no TS was found along the C–O breaking bond in the reaction of protonated *tert*-butanol **13**, as was proposed for the first step of an SN1 reaction (see **TS1** in Scheme 2);[4] and (iv) around of the C···O distance of 1.85 Å, where the reaction of protonated methanol **4** reaches the maximum energy, 8.6 kcal mol^{-1}. The corresponding structure in the scan of the protonated *tert*-butanol **12** has a relatively low energy of only 2.7 kcal mol^{-1}.

The geometries of **TS-6w** and **P2-8**, in which the C···O distance is *ca.* 1.85 Å, are given in Fig. 11, while the geometries of the selected six points of the two scans are given in Fig. S2 in ESI.† At **TS-6w**, the C···O and C···Cl distances are 1.872 and 2.452 Å, respectively, while these distances at **P2-8** of the scan of the reaction of protonated *tert*-butanol **13** are 1.85 and 3.76 Å. When the C···Cl distances are compared with those at the first point of the scans, *i.e.* **P1-6** and **P1-8**, which correspond to the MCs of these reactions, it can be seen that while in the reaction with protonated methanol **4**, this C···Cl distance at **TS-6w** has decreased by 0.78 Å, at **P2-8** of the scan of protonated *tert*-butanol **14** it is shortened by only 0.13 Å. Along the scan of protonated methanol **4**, this distance decreases drastically to 1.80 Å at **P3-6**, while this distance in the reaction path of protonated *tert*-butanol **14** remains at 3.48 Å at **P3-8** (see Fig. S2 in the ESI†). Consequently, the chloride anion clearly does not participate in the reaction path involving *tert*-butanol **14**. Note that **P3-8** corresponds to the proposed intermediate of an S_N1 reaction (see Scheme 2).

The different behaviors of the two scans mainly result from the different stability/reactivity of the methyl **8** and *tert*-butyl **9** carbocations, which are generated along the heterolytic C–O bond breaking. Along the reaction path of protonated *tert*-

butanol **13**, the corresponding carbocation is markedly stabilized by the presence of the three ER methyl groups (see Scheme 4). In addition, the presence of these methyl groups decreases the electrophilic character of the corresponding carbocation with respect to that of methyl carbocation **8** (see Table 2); thus, the *tert*-butyl carbocation **9** does not need the participation of the chloride anion for its stabilization along the reaction path. However, a different behavior is found in the reaction of the methyl carbocation **8**. This carbocation is very unstable, and consequently, it cannot be easily formed. However, along the reaction path, the electrophilic character of the $CH_3\cdots OH_2^+$ species increases, allowing the participation of the nucleophilic chloride anion. This participation demands the approach of this nucleophilic species to the incipient carbocationic center, in such a way that at the corresponding **TS-6w**, the two nucleophilic species, *i.e.*, the chloride anion and the water molecule, strongly stabilize the corresponding methyl carbocation **8**. Thus, the structure of protonate methanol **4** with the C⋯O distance fixed at 1.85 Å has an electrophilicity ω index of 2.15 eV; note that the electrophilicity ω index of $CH_3OH_2^+$ **4** is 1.34 eV (see Table 2). On the other hand, this structure, in which the chloride anion has been removed from **TS-6w**, is 19.9 kcal mol^{-1} higher in energy than protonated methanol **4**. Consequently, the stabilization of 11.7 kcal mol^{-1} found at **TS-6w** can be attributed to the presence of the nucleophilic chloride, which stabilizes the TS by the GEDT.

After passing **TS-6w**, the Cl⋯C distance decreases quickly until the formation of the new Cl–C single bond at methyl chloride **2**, a behavior that does not occur in the reaction of the protonated *tert*-butanol **14** (see Fig. 11 and S2†). Finally, the slight geometric differences found between **TS-6** (see Fig. 4) and **TS-6w** (see Fig. 12) are because both structures were optimized in different solvents, DMSO and water, respectively.

Fig. 12 also shows the sum of the NPA charges in the three frameworks of these selected species. Some interesting conclusions can be obtained from the NPA charges, (i) while the negative charge of the chloride anion remains unchanged on going from the MC to the selected point in the reaction path of protonated *tert*-butanol **14**, along the reaction path on going to **TS-6w**, the chloride anion experiences a loss of 0.20*e* caused by the GEDT occurring towards the electrophilic methyl carbocation **8**; (ii) the positive charge of the methyl carbocation **8** framework at **TS-6w**, 0.49*e*, is lower than that of the *tert*-butyl carbocation of **P2-8**, 0.67*e*, due to the participation of the nucleophilic chloride anion in the former; and finally, (iii) along the two reaction paths, a decrease in the positive charge on the water framework is observed. Note that in the product of the two nucleophilic substitution reactions, the water LG is neutral. The positive charge in the water framework at **TS-6w**, 0.27*e*, is slightly lower than at the selected point of the scan of the reaction of protonated *tert*-butanol **14**, 0.32*e*, as a consequence of the participation of the chloride anion at the TS.

Finally, a comparative ELF topological analysis of the selected points of the scans for the C⋯OH_2 breaking bond in the reactions of protonated methanol **4** and *tert*-butanol **14** was performed. The ELF basin attractor positions are shown in Fig. 13. The first points of both scans show a great similitude; **P1-6** and **P1-8** show the presence of a V(C,O) disynaptic basin integrating 1.56 and 1.59*e*, respectively. Some differences are found between the ELF basin attractor of **TS-6w** and **P2-8**. At both structures, the absence of the V(C,O) disynaptic basins present at **P1-6** and **P1-8** indicates that the rupture of the C–OH_2 bond has already taken place. Both species show the presence of a V(O) monosynaptic basin integrating 1.72 (**TS-6w**) and 1.57*e* (**P2-8**) in the direction of the central carbon. However, while **TS-6w** also shows the presence of a V(Cl) monosynaptic basin integrating 0.55*e* in the direction of the central carbon, **P2-8** does not show any specific V(Cl) monosynaptic basin in this direction. Finally, while the ELF of **P3-6** shows the presence of a V(C,Cl) disynaptic basin integrating 1.24*e*, indicating the formation of the new C–Cl single bond, no V(C,Cl) disynaptic basin is observed at **P3-8**.

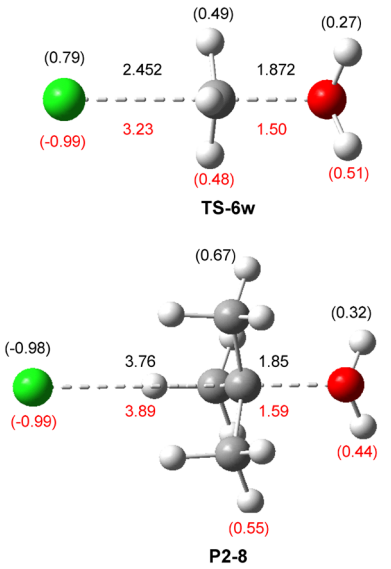

Fig. 12 ωB97X-D/6-311+G(d,p) geometries in water of **TS-6w** and **P2-8**. Distances are given in angstroms Å. The sum of the NPA charges at the three frameworks is given in average number of electrons, *e*. Distances and NPA charges in red correspond to the first point of the scans. The distances of the scan points are given with two decimals.

Thus, while the scan for the C⋯OH_2 breaking bond in the reaction of protonated methanol **4** shows that the rupture of the C–OH_2 has occurred before reaching **TS-6w**, with the formation of the C–Cl bond taking place after it, the scan for protonated *tert*-butanol **14** is associated only with the rupture of the C⋯OH_2 bond. The first parts of both scans are associated with the same chemical event; *i.e.*, the rupture of the C–OH_2 single bond. However, while along the reaction path of protonated *tert*-butanol **13**, the stabilization of the forming tertiary carbocation by the presence of the three ER methyl groups does not demand the participation of the chloride anion, in the case of protonated methanol **4**, it should participate, prompting the S_N2 reaction in a single step.

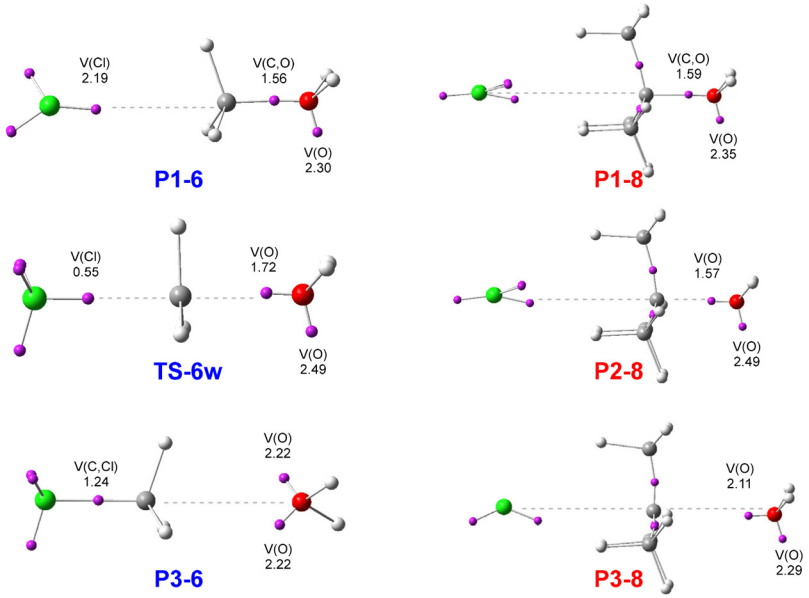

Fig. 13 ωB97X-D/6-311+G(d,p) ELF basin attractor positions and populations of the more significant valence basins of the selected points of the scans for the C···OH_2 breaking bond in the reactions of protonated methanol **4** and *tert*-butanol **14**. Valence basin populations are given in average number of electrons, *e*.

3. Conclusions

Five S_N2 reactions involving methyl monosubstituted compounds and a S_Ni reaction have been studied within MEDT in order to characterize the electronic nature of the TSs involved in these nucleophilic substitution reactions.

Analysis of the electrophilicity ω index at the GS of the reagents indicates that in general, the methyl monosubstituted compounds have a poor tendency to participate in polar reactions with nucleophilic species.

The X···C and C···Y distances at the TSs vary significantly depending on the corresponding C–X and C–Y bond lengths at the GS of the reagents or products. However, an analysis of the H–C–H bond angle at the central methyl framework indicates that, in general, the TSs have a high degree of symmetry in the evolution of the breaking/forming bonds.

Both ELF and QTAIM topological analyses of the electron density at the TSs of the S_N2 and S_Ni reactions indicate that they can be described as the carbocation strongly stabilized by the presence of the neighboring X and Y nucleophilic species. This stabilization is caused by the high GEDT occurring at the TSs, which show a total charge at the methyl group lesser than 0.47*e*.

Finally, a comparative study of the C–O breaking bond in the nucleophilic substitution reactions of *tert*-butanol **12** and methanol **13** with hydrochloric acid allows us to explain the unimolecular and bimolecular nature of the kinetics of these reactions, respectively. In both reactions, a carbocationic species is generated along the initial C–O breaking bond; however, in the case of the *tert*-butyl carbocation **9**, the presence of the three ER methyl groups makes the participation of the chloride anion unnecessary for its stabilization, resulting in a unimolecular mechanism. In the case of methyl carbocation **8**, the strong destabilization and the high electrophilic character of this primary carbocation require the participation of the nucleophilic chloride anion for the C–O breaking bond to be feasible, resulting in a bimolecular mechanism.

The present MEDT study establishes that these S_N2 and S_Ni reactions involve non-concerted breaking/forming bond processes. At the corresponding TSs, the role of the nucleophilic species is to facilitate the departure of the LG by stabilizing the forming methyl carbocation framework. The present study rejects the proposed pentacoordinated TSs for the S_N2 and S_Ni reactions based on the outdated FMO theory.

4. Computational details

This MEDT study has been carried out by performing quantum chemical calculations within Density Functional Theory (DFT).[37] The ωB97X-D[38] functionals, together with the standard 6-311+G(d,p)[39] basis set, which includes diffuses and d-type polarization for second-row elements and p-type polarization functions for hydrogens, were used throughout this MEDT study. The TSs were characterized by the presence of only one imaginary frequency. The Berny method was used in optimizations.[40,41] The intrinsic reaction coordinate[42] (IRC) calculations were performed to establish the unique connection given between the TSs and the corresponding minima.[43,44] Solvent effects were considered by full optimization of the gas phase structures at the same computational level using the polarizable continuum model (PCM)[45,46] in the

framework of the self-consistent reaction field (SCRF),[47–49] and DMSO and water as solvents.

The GEDT[35] values were computed using the equation $GEDT(f) = \sum q_f$, where q are the natural charges[50,51] of the atoms belonging to one of the two frameworks (f) at the TS geometries. Global and local CDFT indices[30,31] were calculated using the equations in ref. 31.

The Gaussian 16 suite of programs was used to perform the calculations.[52] ELF[23] analyses of the ωB97X-D/6-311+G(d,p) monodeterminantal wavefunctions were done by using the TopMod[53] package with a cubical grid of step size of 0.1 Bohr. Molecular geometries and ELF basin attractors were visualized by using the GaussView program.[54]

Data availability

The data supporting this article have been included as part of the ESI.†

Conflicts of interest

The authors declare no conflict of interest.

Acknowledgements

This work has been supported by the Ministry of Science and Innovation (MICINN) of the Spanish Government, project PID2019-110776GB-I00 (AEI/FEDER, UE) and by FONDECYT – Chile through Project No. 1221383 L. R. D. also acknowledges Cooperación Internacional (Fondecyt No. 1221383) by continuous support.

References

1 E. D. Hughes and C. K. Ingold, Mechanism of substitution at a saturated carbon atom. Part IV. A discussion of constitutional and solvent effects on the mechanism, kinetics, velocity, and orientation of substitution, *J. Chem. Soc.*, 1935, **55**, 244–255.
2 E. D. Hughes, Hydrolysis of secondary and tertiary Alkyl Halides, *J. Am. Chem. Soc.*, 1935, **57**, 708–709.
3 J. F. Bunnet, Physical organic terminology. After Ingold, *Bull. Hist. Chem.*, 1996, **19**, 33–42.
4 F. A. Carey and R. J. Sundberg, in *Advanced Organic. Chemistry. Part A: Structure and Mechanisms*, Springer, New York, 2008.
5 K. Fukui, in *Molecular orbitals in chemistry physics and biology*, New York, 1964.
6 M. B. Smith and J. March, in *Advanced organic chemistry: reactions, mechanisms, and structure*, Wiley-Interscience, New York, 6th edn, 2007.
7 S. Shaik, H. B. Schlegel and S. Wolfe, *Theoretical aspects of physical organic chemistry, The SN2 mechanism*, Wiley, New York, 1992.
8 W. P. Hu and D. G. Truhlar, Modeling Transition State Solvation at the Single-Molecule Level: Test of Correlated ab Initio Predictions against Experiment for the Gas-Phase SN2 Reaction of Microhydrated Fluoride with Methyl Chloride, *J. Am. Chem. Soc.*, 1994, **116**, 7797–7800.
9 S. Harder, A. Streitwieser, J. T. Petty and P. V. Schleyer, Ion Pair SN2 Reactions. Theoretical Study of Inversion and Retention Mechanisms, *J. Am. Chem. Soc.*, 1995, **117**, 3253–3259.
10 A. Streitwieser and G. Jayasree, Theoretical Study of the Effect of Coordinating Solvent on Ion Pair SN2 Reactions: The Role of Unsymmetrical Transition Structures, *J. Org. Chem.*, 2007, **72**, 1785–1798.
11 B. L. Kormos and C. J. Cramer, Solvation Effects on Alternative Nucleophilic Substitution Reaction Paths for Chloride/Allyl Chloride and g-Methylated Congeners, *J. Org. Chem.*, 2003, **68**, 6375–6386.
12 S. J. Mo, T. Vreven, B. Mennucci, K. Morokuma and J. Tomasi, Theoretical study of the SN2 reaction of $Cl–(H_2O)+CH_3Cl$ using our own N-layered integrated molecular orbital and molecular mechanics polarizable continuum model method (ONIOM, PCM), *Theor. Chem. Acc.*, 2004, **111**, 154–161.
13 G. Vayner, K. N. Houk, W. L. Jorgensen and J. I. Brauman, Steric Retardation of SN2 Reactions in the Gas Phase and Solution, *J. Am. Chem. Soc.*, 2004, **126**, 9054–9058.
14 S. Giri, E. Echegaray, P. W. Ayers, A. S. Nuñez, F. Lund and A. Toro-Labbé, Insights into the Mechanism of an SN2 Reaction from the Reaction Force and the Reaction Electronic Flux, *J. Phys. Chem. A*, 2012, **116**, 10015–10026.
15 M. Stei, E. Carrascosa, M. A. Kainz, A. H. Kelkar, J. Meyer, I. Szabó, G. Czakó and R. Wester, Influence of the leaving group on the dynamics of a gas-phase SN2 reaction, *Nat. Chem.*, 2016, **8**, 151–156.
16 I. Szabo and G. Czako, Double-Inversion Mechanisms of the $X– + CH_3Y$ [X,Y = F, Cl, Br, I] SN2 Reactions, *J. Phys. Chem. A*, 2015, **119**, 3134–3140.
17 J. Xie and W. L. Hase, Rethinking the SN reaction, *Science*, 2016, **352**, 32–33.
18 M. A. van Bochove, M. Swart and F. M. Bickelhaupt, Nucleophilic substitution at phosphorus (SN2@P): disappearance and reappearance of reaction barriers, *J. Am. Chem. Soc.*, 2006, **128**, 10738–10744.
19 T. A. Hamlin, M. Swart and F. M. Bickelhaupt, Nucleophilic substitution (SN2): dependence on nucleophile, leaving group, central atom, substituents, and solvent, *ChemPhysChem*, 2018, **19**, 1315–1330.
20 S. Pierrefixe, S. J. M. van Stralen, J. N. P. van Stralen, C. Fonseca Guerra and F. M. Bickelhaupt, Hypervalent Carbon Atom: "Freezing" the SN2 Transition State, *Angew. Chem., Int. Ed.*, 2009, **48**, 6469–6471.
21 I. Iribarren, C. Trujillo, G. Sánchez-Sanz, E. Hénon, J. Elguero and I. Alkorta, Influence of Lewis acids on the symmetric SN2 reaction, *Theor. Chem. Acc.*, 2023, **142**, 8.

22 V. Polo, P. González-Navarrete, B. Silvi and J. Andrés, An electron localization function and catastrophe theory analysis on the molecular mechanism of gas-phase identity SN2 reactions, *Theor. Chem. Acc.*, 2008, **120**, 341–349.

23 A. D. Becke and K. E. Edgecombe, A simple measure of electron localization in atomic and molecular systems, *J. Chem. Phys.*, 1990, **92**, 5397–5403.

24 R. Thom, *Structural stability and morphogenesis: an outline of a general theory of models, Benjamin, Reading*, 1975.

25 L. R. Domingo, Molecular Electron Density Theory: A Modern View of Reactivity in Organic Chemistry, *Molecules*, 2016, **21**, 1319.

26 R. F. W. Bader, Y. H. Tang, Y. Tal and F. W. Biegler-König, Properties of atoms and bonds in hydrocarbon molecules, *J. Am. Chem. Soc.*, 1982, **104**, 946–952.

27 R. F. W. Bader, in *Atoms in Molecules: A Quantum Theory*, Oxford University Press, Oxford, New York, 1994.

28 B. Silvi and A. Savin, Classification of chemical bonds based on topological analysis of electron localization functions, *Nature*, 1994, **371**, 683–686.

29 E. Espinosa, I. Alkorta, J. Elguero and E. Molins, From weak to strong interactions: A comprehensive analysis of the topological and energetic properties of the electron density distribution involving X–H···F–Y system, *J. Chem. Phys.*, 2002, **117**, 5529–5542.

30 R. G. Parr and W. Yang, in *Density Functional Theory of Atoms and Molecules*, Oxford, University Press, New York, 1989.

31 L. R. Domingo, M. Ríos-Gutiérrez and P. Pérez, Applications of the Conceptual Density Functional Theory Indices to Organic Chemistry Reactivity, *Molecules*, 2016, **21**, 748.

32 L. R. Domingo and M. Ríos-Gutiérrez, in *Application of Reactivity Indices in the Study of Polar Diels-Alder Reactions. Conceptual Density Functional Theory: Towards a New Chemical Reactivity Theory*, ed. S. Liu, WILEY-VCH GmbH, 2022, vol. 2, pp. 481–502.

33 M. Ríos-Gutiérrez, A. Saz Sousa and L. R. Domingo, Electrophilicity Nucleophilicity Scales at Different Computational Levels, *J. Phys. Org. Chem.*, 2023, e4503.

34 P. Jaramillo, L. R. Domingo and P. Pérez, Towards an intrinsic nucleofugality scale. The leaving group (LG) ability in CH_3LG model system, *Chem. Phys. Lett.*, 2006, **420**, 95–99.

35 L. R. Domingo, A New C-C Bond Formation Model Based on the Quantum Chemical Topology of Electron Density, *RSC Adv.*, 2014, **4**, 32415–32428.

36 L. R. Domingo and M. Ríos-Gutiérrez, Revealing the Decisive Role of Global Electron Density Transfer in the Reaction Rate of Polar Organic Reactions within Molecular Electron Density Theory, *Molecules*, 2024, **29**, 1.

37 P. Hohenberg and W. Kohn, Inhomogeneous Electron Gas, *Phys. Rev.*, 1964, **136**, B864–B871.

38 J.-D. Chai and M. Head-Gordon, Long-range corrected hybrid density functionals with damped atom–atom dispersion corrections, *Phys. Chem. Chem. Phys.*, 2008, **10**, 6615–6620.

39 M. J. Hehre, L. Radom, P. v. R. Schleyer and J. People, in *Ab initio Molecular Orbital Theory*, Wiley, New York, 1986.

40 H. B. Schlegel, Optimization of equilibrium geometries and transition structures, *J. Comput. Chem.*, 1982, **3**, 214–218.

41 H. B. Schlegel, in *Modern Electronic Structure Theory*, ed. D. R. Yarkony, World Scientific Publishing, Singapore, 1994.

42 K. Fukui, Formulation of the reaction coordinate, *J. Phys. Chem.*, 1970, **74**, 4161–4163.

43 C. González and H. B. Schlegel, Reaction path following in mass-weighted internal coordinates, *J. Phys. Chem.*, 1990, **94**, 5523–5527.

44 C. González and H. B. Schlegel, Improved algorithms for reaction path following: Higher–order implicit algorithms., *J. Chem. Phys.*, 1991, **95**, 5853–5860.

45 J. Tomasi and M. Persico, Molecular interactions in solution: and overview of methods based on continuous distributions of the solvent, *Chem. Rev.*, 1994, **94**, 2027–2094.

46 B. Ya Simkin and I. I. Sheikhet, *Quantum chemical and statistical theory of solutions–computational approach*, Ellis Horwood, London, 1995.

47 M. Cossi, V. Barone, R. Cammi and J. Tomasi, Ab initio study of solvated molecules: A new implementation of the polarizable continuum model, *Chem. Phys. Lett.*, 1996, **255**, 327–335.

48 E. Cances, B. Mennucci and J. Tomasi, A new integral equation formalism for the polarizable continuum model: Theoretical background and applications to isotropic and anisotropic dielectrics, *J. Chem. Phys.*, 1997, **107**, 3032–3041.

49 V. Barone, M. Cossi and J. Tomasi, Geometry optimization of molecular structures in solution by the polarizable continuum model, *J. Comput. Chem.*, 1998, **19**, 404–417.

50 A. E. Reed, R. B. Weinstock and F. Weinhold, Natural population analysis, *J. Chem. Phys.*, 1985, **83**, 735–746.

51 A. E. Reed, L. A. Curtiss and F. Weinhold, Intermolecular interactions from a natural bond orbital, donor-acceptor viewpoint, *Chem. Rev.*, 1988, **88**, 899–926.

52 M. J. Frisch, *et al.*, *Gaussian 16*, Gaussian, Inc., Wallingford, CT, 2016.

53 S. Noury, X. Krokidis, F. Fuster and B. Silvi, Computational tools for the electron localization function topological analysis, *Comput. Chem.*, 1999, **23**, 597–604.

54 R. Dennington, T. A. Keith and J. M. Millam, *GaussView, Version 6.1*, Semichem Inc., Shawnee Mission, KS, 2016.